Environ. Sci. Technol. **2006**, *40,* 1843−1848

Chemistry of Particle Inception and Growth during α-Pinene Ozonolysis

MICHAEL P. TOLOCKA,[†]
KATHERINE J. HEATON,
MATTHEW A. DREYFUS, SHENYI WANG,
CHRISTOPHER A. ZORDAN,
THOMAS D. SAUL, AND
MURRAY V. JOHNSTON*

Department of Chemistry and Biochemistry, University of Delaware, Newark, Delaware 19716

A flow-tube reactor was used to study the formation of particles from α-pinene ozonation. Particle phase products formed within the first 3−22 s of reaction were analyzed on-line using a scanning mobility particle sizer and two particle mass spectrometers. The first, a photoionization aerosol mass spectrometer (PIAMS), was used to determine the molecular composition of nascent particles between 30 and 50 nm in diameter. The second, a nano-aerosol mass spectrometer (NAMS), was used to determine the elemental composition of individual particles from 50 nm to below 10 nm in diameter. Molecular composition measurements with PIAMS confirm that both the stabilized Criegee intermediate and hydroperoxide channels of α-pinene ozonolysis are operative. However, these channels alone cannot explain the high oxygen content of the particles measured with NAMS. The carbon-to-oxygen mole ratios of suspected nucleating agents are in the range of 2.25−4.0, while the measured ratios are from 1.9 for 9 nm particles to 2.5 and 2.7 for 30 and 50 nm particles, respectively. The large oxygen content may arise by co-condensation of small oxygenated molecules such as water or multistep reactions with ozone, water, or other species that produce highly oxygenated macromolecules. In either case, the increasing ratio with increasing particle size suggests that the aerosol becomes less polar with time.

Introduction

In 1960, Went observed that the blue haze in forested areas results from emitted biogenic species that form aerosols, which efficiently scatter shorter wavelengths of light (*1*). Particles that are formed from biogenic emissions provide surfaces for heterogeneous reactions in the atmosphere and influence the earth's energy balance directly by scattering radiation and indirectly by serving as cloud condensation nuclei (*2*, *3*). The reaction of biogenic monoterpenes such as α-pinene with ozone gives a variety of multifunctional oxygenated products. Of these, dicarboxylic acids such as *cis*-pinonic acid or pinic acid have been suggested as the primary building blocks for particles based on their low vapor pressures (*4*). Indeed, nucleation events in remote, forested areas of Finland have been shown to produce organic particles whose constituents have similar butanol solubility as these compounds (*5*). Nonetheless, it has been argued that the physicochemical properties of these and other primary products of α-pinene oxidation are insufficient for new particle formation (*6*). For this reason, recent work in our laboratory and elsewhere has focused on the formation of oligomeric species that may assist the partitioning of organic matter to the particle phase (*7*−*16*).

The two main reaction channels proposed for the formation of secondary organic aerosol from α-pinene ozonolysis and some noteworthy primary products are shown in Figure 1. Thermally stabilized Criegee intermediates (SCIs) have been proposed based on the reduction in particle formation by scavenging these intermediates with water and other low molecular weight compounds (*9*, *10*, *17*). It has been proposed that new particle formation occurs through this channel by the formation of low-volatility products such as secondary ozonides from reaction of the SCI with an aldehyde, also shown in Figure 1, or through the addition of acids across the SCI forming the hydroperoxy ester (*10*). The formation of low volatility species through the hydroperoxide channel has been proposed based on the reduction in particle formation by OH scavengers and chemical measurements on collected aerosol, including iodometric titration and mass spectrometry (*11*, *12*). In this case, new particle formation would likely occur through the formation of peroxidic oligomers, which have been detected in laboratory experiments (*13*−*15*) and have been suggested in modeling studies (*17*). While peroxides can also be formed through the SCI channel, it has been argued that the SCI channel is less likely to contribute to new particle formation, because the SCI should react primarily with water vapor under atmospheric conditions (*11*, *18*). Recent results show that increasing relative humidity increases the aerosol number and mass yield for a variety of biogenic species ozonations (*19*).

We report here chemical composition measurements of particles in the 9−50 nm size range that are produced within the first few seconds of reaction. Oligomeric species detected in these particles confirm that both the stabilized Criegee intermediate and hydroperoxide channels of α-pinene ozonolysis are operative. However, these channels alone cannot explain the high oxygen content of the particles, which suggests that the mechanism of particle formation is more complex than previously thought.

Experimental Section

Particle formation and growth was performed in a concentric flow-tube reactor that is similar to one used previously for heterogeneous kinetics (*20*). Ozone was generated and analyzed with a commercial generator (Thermo Electron Corporation, model 49C). α-Pinene vapor was produced by passing a small air flow over the liquid and then diluting it with additional air. Dry (RH < 5%), filtered air with a particle number concentration below 20 cm^{-3} was used. The conditions for the four specific experiments studied in this work are given in Table 1. For most experiments, the ozone and α-pinene flows were mixed under laminar flow conditions ($Re = 150$). After mixing, the ozone concentration was 1.0 ppm (measured in the absence of α-pinene in the apparatus). The current experimental setup does not have the ability to directly measure the α-pinene concentration. For this reason, the α-pinene concentrations given in Table 1 are upper limits based on the assumption that the vapor passing over the liquid becomes saturated. It is likely that the true α-pinene concentrations are one-half to one-third of their stated values. The concentrations in Table 1 overlap the range studied in other experiments, for example, ref *10*. Two different flow-

* Corresponding author phone: (302)831−8014; fax: (302)831−6335; e-mail: mvj@udel.edu.
[†] Current affiliation: Department of Chemistry, University of North Carolina, Chapel Hill, North Carolina.

10.1021/es051926f CCC: $33.50 © 2006 American Chemical Society
Published on Web 02/11/2006

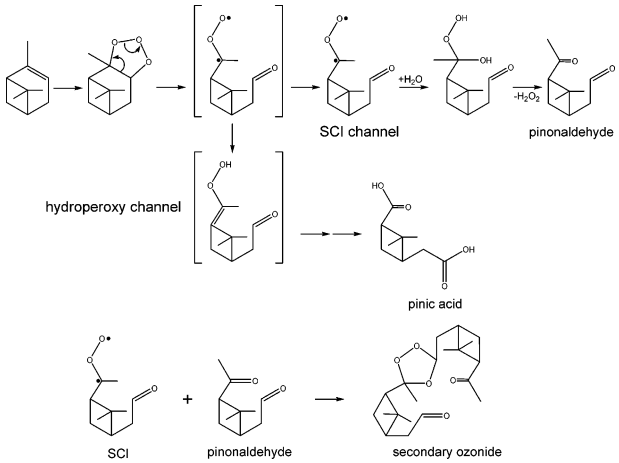

FIGURE 1. (Top) Stabilized Criegee intermediate (SCI) and hydroperoxide reaction channels for α-pinene ozonolysis are summarized. Also shown are two prominent primary products. Bracketed species indicate excited-state intermediates. (Bottom) Reaction of the SCI with pinonaldehyde to give a secondary ozonide.

tube lengths were used, giving residence times after mixing of either 3 or 22 s (calculated from the volumetric flow rates of the reactants into the tube).

The reactant concentrations used in this work (Table 1) were chosen to generate particles over the size range of interest (<10−50 nm diameter) while at the same time providing sufficiently large and stable concentrations for repeated measurements with the particle mass spectrometers. The "30" and "50" nm experiments were performed under the same reactant concentration and flow conditions, differing only in the flow-tube length, i.e., reaction time. The "43" nm experiment was performed under the same reactant flow conditions and tube length as the "50" nm experiment, except that the α-pinene concentration was lowered by an order of magnitude. This lower concentration produced lower number and mass concentrations of aerosol and a smaller mean particle diameter, all presumably because the nucleation and growth rates were slower. The experimental conditions in the "22" nm experiment were studied because they gave a sufficient number concentration in the 9 nm diameter range to permit single-particle measurements with electrodynamic focusing (see below). For this experiment only, the linear velocities of the α-pinene and ozone flows were not matched (30% difference), which may have resulted in nonlaminar flow due to Kelvin−Helmoltz instabilities in the reaction tube. Turbulence in the flow reactor, though, may have little effect on the observed kinetics (*10*). The aerosol yields (*21*) defined here as the amount of aerosol formed normalized by the ozone concentration change (because it is the limiting reactant) increase from 0.066% for the 22 nm experiment to 6.1% for the 50 nm experiment, similar to the yields reported by other groups (*17*, *22*).

Particle size distributions were measured with a nano scanning mobility particle sizer (SMPS, model 3080 classifier equipped with a Po-210 neutralizer with short mobility tube and model 3025A ultrafine condensation particle counter; TSI, Inc., St. Paul, MN) attached to the exit of the flow tube. Two separate checks were made to ensure that the measured size distributions were correct. First, the length of the sampling line from the flow reactor to the SMPS was increased to double the expected residence time in the SMPS system. This increase resulted in no measurable change in the size distribution. Second, the absolute signal intensities of the multiply charged ions in the mass spectra of nominally 9, 30, and 50 nm diameter particles from α-pinene ozonolysis taken with the nano-aerosol mass spectrometer (NAMS, see below) were compared. The absolute intensities increase monotonically with increasing particle size, as observed in other laboratories (*23*−*25*). Furthermore, they are comparable to those obtained with our instrument using standard particles (sucrose particles generated with a TSI electrospray generator) of similar size. The consistency of the SMPS and NAMS data suggests that the size distributions measured by the SMPS are correct.

Two methods were used to provide complementary chemical information of the nascent, ultrafine particles. The first, a photoionization aerosol mass spectrometer (PIAMS), provides molecular information and is discussed in detail elsewhere (*26*, *27*). Particles entering the mass spectrometer are collected on a cooled probe and irradiated with an infrared laser, and the desorbed molecules are photoionized with vacuum ultraviolet radiation. Recently, this method has been used to study combustion particle inception and growth in a premixed laminar flame (*27*) and the kinetics of cholesterol particle ozonolysis (*15*).

The second, a nano-aerosol mass spectrometer (NAMS), provides elemental composition of individual particles. Particles above ∼30 nm in diameter are efficiently transferred through an aerodynamic inlet into the mass spectrometer source region. Analysis is performed by free-firing the ablation laser (see below) to randomly "hit" particles that happen to be in the laser beam path when the laser fires. This approach was used to analyze nascent particles in the 30, 43, and 50 nm experiments. Particles below ∼30 nm in diameter are not efficiently transferred to the mass spectrometer region and must be electrodynamically focused through the inlet and trapped in the source region in order to achieve an adequate hit rate. The focusing and trapping steps are size (or more precisely m/z) dependent and allow a specific size range to be selected from a broad distribution. This approach was used to select and analyze ca. 9 nm particles in the 22 nm experiment. Initially, the aerosol is brought to an equilibrium charge distribution by passing through a polonium (Po-210) aerosol neutralizer. Particles then enter the mass spectrometer through an aerodynamic inlet. After exiting the critical orifice, charged particles in the distribution are focused through a quadrupole ion lens and trapped in a 3-dimensional quadrupole ion trap. Trapped particles are ablated with a tightly focused (75 mm f.l.) high power laser beam (532 nm, 170 mJ). When a particle is in the focused laser beam, a plasma is formed which vaporizes the particle and converts its contents into multiply charged positive ions. The radio frequency potentials of the ion lens and trap used in this work were (136 kHz, 1340 V p−p) and (125 kHz, 2200 V p−p), respectively, as measured with a Tectronics P6105 probe. Using these parameters to analyze sucrose nanoparticles that are size-selected with the nano SMPS, it is found that the median particle diameter analyzed was 9.5 nm with $\sigma_g = 1.1$. For the 22 nm experiment of α-pinene ozonolysis, particles were hit only when the focusing and trapping potentials were applied. In other words, under the conditions of this experiment there was no measurable background hit rate from unfocused and/or uncharged particles. Only charged particles in the 9.5 nm size range were detected.

Carbon-to-oxygen (C/O) mole ratios were obtained by dividing the C^{2+}, C^{3+}, and C^{4+} signal intensities by the respective O^{2+}, O^{3+}, or O^{4+} signal intensities. The three C/O mole ratios (C^{2+}/O^{2+}, C^{3+}/O^{3+}, and C^{4+}/O^{4+}) obtained from each sample were then averaged together to obtain a single C/O mole ratio for each particle size. Singly charged ions were not included because of a background signal at these m/z values. Since the C^{3+} and O^{4+} peaks overlap, their relative contributions were deconvoluted assuming that $C^{2+}/O^{2+} = C^{3+}/O^{3+} = C^{4+}/O^{4+}$. This assumption appears to be valid because the ionization potentials for $C^{2+} \approx O^{2+}$, $C^{3+} \approx O^{3+}$, and $C^{4+} \approx O^{4+}$. When this approach is used to analyze standard particles of known composition (sucrose) over the

TABLE 1. Reaction Conditions and Particle Size Distributions[a]

mean particle diameter (nm)	α-pinene concentration (ppm)	ozone concentration (ppm)	reaction time (s)	dN/d(log d_p) at mean particle diameter	σ_g	aerosol concentration (particles/cm^3)	aerosol concentration (μg/m^3)
22[b,c]	83	1	3	1.6×10^6	1.6	6.5×10^5	15
43	11	1	22	8.6×10^6	1.3	2.1×10^6	95
30	136	1	3	1.2×10^7	1.4	4.0×10^6	36
50	136	1	22	2.2×10^7	1.3	5.9×10^6	400

[a] The measured values vary less than ±10% during the course of an experiment. Note that the α-pinene concentrations were not measured and the values given are upper limits. [b] Particles selected for analysis from this distribution by electrodynamic focusing had a median diameter of 9.5 nm and $\sigma_g = 1.1$, as determined from laboratory-generated sucrose particles. dN/d(log d_p) at 9.5 nm was 2.1×10^5. [c] The linear velocities of the α-pinene and ozone flows were not matched (30% difference) in this experiment. In all other experiments, the two flow velocities were matched.

size range of the α-pinene ozonolysis experiment (8−50 nm diameter), the measured C/O ratios are within ±20% of the expected C/O ratio. For each aerosol distribution in this work, the reported C/O ratios are the average of the results from at least seven separate experiments, with the spectrum from each experiment being the average of 50 single-particle spectra. The relative standard deviations of the measured C/O ratios were <15%.

Results and Discussion

The experimental conditions investigated in this work are summarized in Table 1. The reaction conditions of the 30 and 50 nm experiments differ only in reaction time, which allows changes in the chemistry associated with particle growth in this size range to be studied. As Table 1 shows, the particle number concentrations of the two experiments are similar while the size distribution and corresponding mass concentration of the longer reaction time aerosol are shifted to larger values. The reaction conditions of the 43 and 50 nm experiments differ only in the initial α-pinene concentration. These experiments give insight into the role that the α-pinene concentration plays in the chemistry of particle formation and growth. As might be expected, decreasing the α-pinene concentration uniformly decreases the number concentration, mass concentration, and mean particle diameter of the aerosol. The reaction conditions of the 22 nm experiment are significantly different from those of the rest. The conditions adopted here were chosen to generate a sufficient number of particles in the 9 nm size range so that the chemical composition of particles in this earlier stage of growth could be investigated. Although other combinations of reaction conditions were found to produce particles in this size range, either the number concentration and size range of the aerosol were not reproducible over time or the number concentration was too small.

Parts a and b of Figure 2 show the PIAMS spectra of particles sampled during the 43 and 50 nm experiments, respectively. In each experiment, a polydisperse aerosol is produced with a mean particle diameter (d_p) as specified. Because of the different mass concentrations of the two aerosols (Table 1), the 43 nm spectrum was obtained by collecting aerosol for 20 min, while the 50 nm spectrum was obtained by collecting aerosol for 10 min. In the 150−200 m/z region, the mass spectra look remarkably similar to that reported by Docherty et al. (*11*), with prominent peaks observed at 169, 183, 185, and 199 m/z. These ions have been assigned as fragments of higher molecular weight oligomers produced through the hydroperoxide channel (*11*, *12*). Possible building blocks for these oligomers include pinonic acid (MW = 184), pinic acid (MW = 186), and 10-hydroxypinonic acid (MW = 200). Also observed in Figure 2 are ions at 310, 324, 338, 352, 366, 380, and 394 m/z, which have not been reported in previous studies. The 352 m/z species corresponds to a secondary ozonide (*10*, *28*) formed by the addition of *cis*-pinonaldehyde, a common gas-phase product

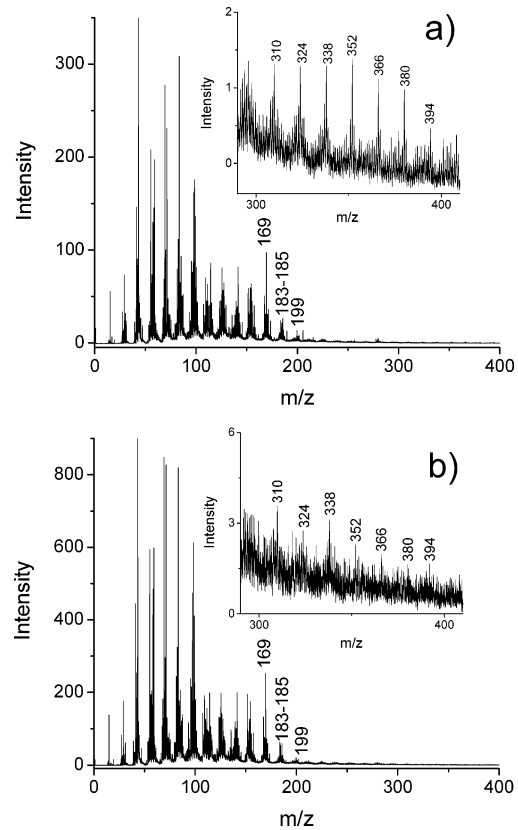

FIGURE 2. Laser desorption−vacuum ultraviolet photoionization mass spectra of particles produced by the reaction of α-pinene with ozone. In (a), the 43 nm aerosol was sampled into the mass spectrometer for a 20 min period; in (b), the 50 nm aerosol was sampled into the mass spectrometer for a 5 min period.

observed in this reaction, to the SCI (see Figure 1) (*29*−*31*). Similarly, the species observed at 338 and 324 m/z correspond to secondary ozonides formed by the additions of other gas-phase products, norpinonaldehyde and 2,2-dimethylcyclobutane-1,3-dicarboxyaldehyde, respectively, to the SCI.

Other routes for formation of the high m/z products in Figure 2 involve the addition and/or subtraction of small oxygenated species. For example, each of the following reactions generates a 352 Da molecular mass product:

$$\text{SCI} + \text{pinic acid} - H_2O \quad (\text{product MW} = 352)$$

$$\text{SCI} + \text{SCI} + H_2O - H_2O_2 \quad (\text{product MW} = 352)$$

The first reaction involves addition of pinic acid to the SCI followed by dehydration either in the condensed phase during particle growth or during the desorption ionization process. (A similar reaction sequence involving the addition of 10-hydroxypinonic acid to the SCI followed by dehydration to

the vinyl ester would give a product of 366 Da, which is also observed in Figure 2.) Reaction of the SCI with acids (pinic, pinonic, and 10-hydroxypinonic) is thought to be kinetically favorable at atmospheric conditions (*10*). The second reaction could proceed by the addition of water to the SCI followed by reaction with another SCI, or by self-reaction of the SCI to form a 1,2,4,5-tetraoxane (*29*, *31*−*33*),

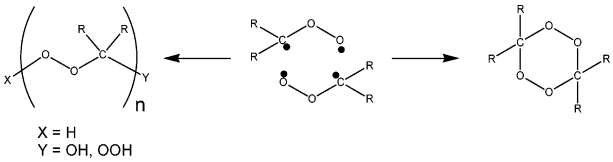

or a linear peroxidic species capped by the addition of water (*31*). Again, the elimination of hydrogen peroxide yields the final product. The series of ions in the high m/z region of Figure 2 could also arise from the combined addition/subtraction of several small oxygenated species:

$$2H_2O - H_2CO - H_2O_2 \qquad \text{mass difference} = 28 \text{ Da}$$

Both formaldehyde and hydrogen peroxide are known products of α-pinene ozonolysis (*17*). They could be eliminated from an SCI-addition product after the addition of water to form a lower-mass species (e.g., 352 → 324 and 338 → 310), or the reverse reaction could occur where the formaldehyde and hydrogen peroxide eliminated from other species are added to the SCI-addition product to form a higher-mass species after the elimination of water (e.g., 352 → 380, 338 → 366, and 366 → 394). In any case, the SCI-addition product is likely to be a reactive species.

When interpreting PIAMS spectra, it is important to distinguish molecular decomposition, which occurs in a high-pressure environment where numerous molecular collisions occur prior to mass analysis, from ion fragmentation, which occurs under collision-free conditions in the high-vacuum region of the mass analyzer. Molecular decomposition can occur in situ as an aerosol-phase reaction or during the desorption step of product analysis in the PIAMS. In either case, molecular collisions accompanying the decomposition lead to formation of "stable" even-electron products that, when ionized, give odd-electron, even-m/z ions. The high-m/z ion series 310, 324, 338, ... would fall into this category. Ion fragmentation inside the mass spectrometer generally leads to even-electron, odd-m/z ions. The lower-m/z ion group (169, 183, 185, 199) would fall into this category.

It is significant that ions corresponding to the *direct addition* of aldehydes to the SCI are observed, while those of the acids are not. In the atmosphere, the organic precursor concentration is much smaller than the levels studied here. While the rate coefficient for reaction of the SCI with water is much lower than that for reaction with any corresponding organic molecule, the reaction rate of the SCI with water to produce the [α]-hydroperoxy alcohol should be competitive owing to the high water vapor concentration (*14*, *34*). While some calculations and measurements suggest that the primary decomposition pathway of the [α]-hydroperoxy alcohol is to the acid and hydroxyl radical (*35*, *36*), others have measured that this pathway accounts for <30% of the observed products (*18*, *37*). Rather, the major products were found to be H_2O_2 and the aldehyde, in this case, pinonaldehyde. It appears that water clusters may play a crucial role in the thermochemistry (*38*, *39*) of secondary ozonide formation by lowering of the transition state of the aldehyde channel. Note that the direct oxidation of α-pinene through the OH channel may also produce significant amounts of pinonaldehyde (*40*). Taken together, both the OH and O_3 oxidation channels could facilitate secondary ozonide formation with the pinonaldehyde and other aldehydes, even though their rate coefficients for reaction with the SCI are expected to be lower than those of the corresponding acids.

It is also possible that the absence of SCI + acid products in Figure 2 reflects PIAMS detection efficiencies. The SCI + aldehyde products are less polar than the SCI + acid products and, therefore, more likely to withstand desorption and ionization, giving even-m/z ions corresponding to the appropriate molecular masses. The SCI + acid products could undergo molecular decomposition during the desorption step to produce less-polar, more-volatile products which are subsequently ionized and detected as even-m/z ions. Or they may be vaporized intact, but the internal energy is so high that ion fragmentation occurs to produce odd-m/z ions. While the mass spectra in Figure 2 may give only a partial view of the species present in these particles, comparing spectra from the different experiments in Table 1 gives significant insight into the chemical processes involved. Note that these species, whether secondary ozonides or hydroxy esters, will decompose into acids and aldehydes upon thermolysis (*41*, *42*), which can explain their absence from previous off-line GC-MS analysis studies (*43*).

The 43 nm spectrum in Figure 2a, the 50 nm spectrum in Figure 2b, and the corresponding 30 nm spectrum (not shown) are very similar, showing the same set of prominent ions in the 169−199 and 310−394 m/z regions. Furthermore, the peak area ratios of ions in the higher-m/z region to those in the lower-m/z region (352/199, 338/199, 352/185, etc.) are the same within experimental error. (While the signal-to-noise ratio of the high-m/z ions is greater in Figure 2a than in Figure 2b, the peak area ratios, e.g., 352/199, etc., are the same.) This observation leads to two conclusions: first, that the chemical species involved in particle growth across the 30−50 nm region are similar, and second, that the chemical species involved are not strongly dependent on α-pinene concentration in the 10−100 ppm range. The spectra in Figure 2 reconcile the divergent results of previous studies by providing direct molecular evidence for both the SCI and hydroperoxide channels in the formation of secondary aerosol. While molecular-mass spectrometry is able to identify chemical species that are characteristic of specific reaction pathways, as discussed above it does not necessarily provide a complete view of particle composition. For this reason, complementary measurements are highly desirable. In the present study, the atomic composition of the aerosol is determined by NAMS.

Figure 3 shows the NAMS spectra of 9, 30, and 50 nm particles. (The 43 nm aerosol could not be characterized by NAMS because the particle number concentration was too small to achieve an acceptable hit rate.) For the two larger particle sizes, the electrodynamic focusing and trapping capabilities of NAMS were disabled and each polydisperse aerosol was analyzed in its entirety. The 9 nm data were obtained from the 22 nm experiment with the focusing and trapping capabilities enabled so that only particles in a narrow size range were analyzed (median diameter = 9.5 nm, σ_g = 1.1), although much larger particles were generated ($d_{p,avg}$ = 22 nm, σ_g = 1.7). Particle vaporization and ionization results in the formation of multiply charged ions whose relative intensities give the elemental composition. In Figure 3, multiply charged carbon (3, 4, and 6 m/z) and oxygen (4, 5.3, and 8 m/z) are observed, as is hydrogen (1 m/z). No other multiply charged ions are observed, confirming that the particles contain only carbon, oxygen, and hydrogen.

The carbon-to-oxygen (C/O) mole ratio, obtained from the relative signal intensities in the mass spectra, increases from 1.9 for 9 nm particles to 2.5 for 30 nm particles and 2.7 for 50 nm particles. The 30 and 50 nm results are the same within the precision of the measurement (±15%). The C/O

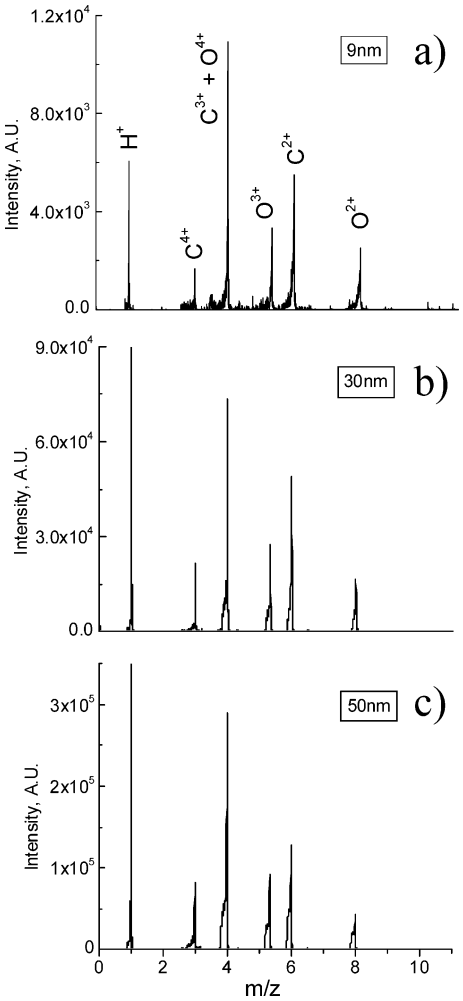

FIGURE 3. High-energy laser ablation mass spectra of (a) 9, (b) 30, and (c) 50 nm diameter particles produced by the reaction of α-pinene with ozone. Each spectrum is the average of 50 single-particle mass spectra. Note that the absolute signal intensity increases with increasing particle size.

ratios for all three particle sizes are lower than anticipated, as the C/O mole ratios of most gas-phase products of α-pinene ozonolysis are much higher, for example, C/O = 5.0 for pinonaldehyde (Figure 1). Indeed, incorporation of one ozone molecule into the α-pinene precursor structure gives at most three oxygen atoms (C/O = 3.3). The hydroperoxide channel can give lower C/O ratios through multistep processes that remove a carbon atom and/or add one or more oxygen atoms, with the most favorable example being C/O = 2.25 for pinic acid (Figure 1). Not surprisingly, secondary ozonides and hydroperoxy esters produced by reaction of the SCI with all major gas-phase products including pinic acid give C/O ratios that are higher than those for the aerosol. Oligomer formation tends to proceed by the elimination of H_2O or other small molecules that decreases the oxygen content.

If so many molecular products have large C/O ratios, how might lower C/O ratios arise? There are two main possibilities. First, small molecules such as H_2O or H_2O_2, the latter of which is a byproduct of α-pinene ozonolysis, may co-condense with the nucleating compounds to lower the effective C/O ratio of the particles (*44*). As with binary sulfuric acid−water nucleation, these molecules may facilitate aerosol formation by lowering the free-energy barrier to growth provided that they do not react with intermediates in the reaction sequence to form the nucleating compounds. Alternatively, water may efficiently condense on a nanoparticle core composed of highly polar, water-soluble organic matter (*45*). (While the air used in these experiments was nominally dry, a sufficient amount of water vapor may be present, even though it is below the detection limit of the hygrometer.) A second possibility is direct, chemical incorporation of oxygen into the molecular structure of the nucleating compounds. Reactions of intermediates with HCHO, HCOOH, H_2O, H_2O_2, HO_2, O_2, or the like have been suggested for both the SCI and the hydroperoxide channels (*11*, *18*). These sequences generally require many steps and may not have time to occur in the short time frame of a flow-tube reactor. Alternatively, it is possible that the vinyl hydroperoxide produced early in the hydroperoxide channel (Figure 1) reacts with an additional ozone molecule, allowing more oxygen atoms to be incorporated per α-pinene precursor molecule.

While these possibilities cannot be distinguished at this point, it is clear that oxygen plays a greater role in the early stage of particle growth than might be inferred from molecular mass spectrometry alone, highlighting the need for future investigation. The increasing C/O ratio with increasing particle size suggests that the aerosol becomes less polar with time. This observation is consistent with a higher degree of polymerization in large particles, because oligomer formation tends to decrease the oxygen content. Indeed, in at least one study, the oligomer content has been shown to increase as the aerosol ages (*16*). It may be necessary in future work to distinguish small and perhaps highly polar oligomers that induce new particle formation from large, less polar oligomers that facilitate particle growth.

Acknowledgments

This research was supported by grants from the National Science Foundation (CHE-0517972) and the United States Environmental Protection Agency (R829622010 and RD83216601). Although the research described in this article was funded in part by the U.S.E.P.A., it has not been subjected to the Agency's required peer and policy review; therefore, it does not necessarily reflect the views of the Agency, and no official endorsement should be inferred. The authors acknowledge Richard Kamens for discussions and preprints.

Literature Cited

(1) Went, F. W. Blue hazes in the atmosphere. *Nature* **1960**, *187*, 641−643.

(2) Pandis, S. N.; Harley, R. A.; Cass, G. R.; Seinfeld, J. H. Secondary Aerosol Formation and Transport. *Atmos. Environ.* **1992**, *26A* (13), 2269−2282.

(3) Ravishankara, A. R. Heterogeneous and multiphase chemistry in the troposphere. *Science* **1997**, *276*, 1058−1064.

(4) Jenkin, M. E.; Shallcross, D. E.; Harvey, J. N. Development and application of a possible mechanism for the generation of cis-pinic acid from the ozonolysis of [alpha]- and [beta]-pinene. *Atmos. Environ.* **2000**, *34* (18), 2837−2850.

(5) O'Dowd, C. D.; Aalto, P.; Hmeri, K.; Kulmala, M.; Hoffmann, T. Aerosol formation: Atmospheric particles from organic vapors. *Nature* **2002**, *416*, 497−498.

(6) Zhang, K. M.; Wexler, A. S. A hypothesis for growth of fresh atmospheric nuclei. *J. Geophys. Res.* **2002**, *107* (D21), AAC-15/1−15/6.

(7) Tolocka, M. P.; Jang, M.; Ginter, J. M.; Cox, F. J.; Kamens, R.; Johnston, M. V. Formation of oligomers in secondary organic aerosol. *Environ. Sci. Technol.* **2004**, *38* (5), 1428−1434.

(8) Gao, S.; Keywood, M.; Ng, N. L.; Surratt, J.; Varutbangkul, V.; Bahreini, R.; Flagan, R. C.; Seinfeld, J. H. Low-molecular-weight and oligomeric components in secondary organic aerosol from the ozonolysis of cycloalkenes and [alpha]-pinene. *J. Phys. Chem. A* **2004**, *108*, 10147−10164.

(9) Bonn, B.; Schuster, G.; Moortgat, G. K. Influence of water vapor on the process of new particle formation during monoterpene ozonolysis. *J. Phys. Chem. A* **2002**, *106* (12), 2869−2881.

(10) Lee, S.; Kamens, R. M. Particle nucleation from the reaction of [alpha]-pinene and O_3. *Atmos. Environ.* **2005**, *39*, 6822−6832.

(11) Docherty, K. S.; Wu, W.; Lim, Y. B.; Ziemann, P. J. Contributions of organic peroxides to secondary aerosol formed from reactions of monoterpenes with O_3. *Environ. Sci. Technol.* **2005**, *39* (11), 4049−4059.
(12) Docherty, K. S.; Ziemann, P. J. Effects of stabilized Criegee intermediate and OH radical scavengers on aerosol formation from reactions of [beta]-pinene with O_3. *Aerosol Sci. Technol.* **2003**, *37* (12), 877−891.
(13) Tobias, H. J.; Ziemann, P. J. Thermal desorption mass spectrometric analysis of organic aerosol formed from reactions of 1-tetradecene and O_3 in the presence of alcohols and carboxylic acids. *Environ. Sci. Technol.* **2000**, *34*, 2105−2115.
(14) Tobias, H. J.; Docherty, K. S.; Beving, D. E.; Ziemann, P. J. Effect of relative humidity on the chemical composition of secondary organic aerosol formed from reactions of 1-tetradecene and O_3. *Environ. Sci. Technol.* **2000**, *34*, 2116−2125.
(15) Dreyfus, M. A.; Tolocka, M. P.; Dodds, S.; Dykins, J.; Johnston, M. V. Cholesterol ozonolysis: Kinetics, mechanism, and oligomer products. *J. Phys. Chem. A* **2005**, *109*, 6242−6248.
(16) Kalberer, M.; Paulsen, D.; Sax, M.; Steinbacher, M.; Dommen, J.; Prevot, A. S. H.; Fisseha, R.; Weingartner, E.; Frankevich, V.; Zenobi, R.; Baltensperger, U. Identification of polymers as major components of atmospheric organic aerosols. *Science* **2004**, *303*, 1659−1662.
(17) Kamens, R.; Jang, M.; Chien, C.-J.; Leach, K. Aerosol formation from the reaction of [alpha]-pinene and ozone using a gas-phase kinetics-aerosol partitioning model. *Environ. Sci. Technol.* **1999**, *33* (9), 1430−1438.
(18) Hasson, A. S.; Chung, M.; Kuwata, K.; Converse, A. D.; Krohn, D.; Paulson, S. E. Reaction of Criegee intermediates with water vapor—An additional source of OH radicals in alkene ozonolysis? *J. Phys. Chem. A* **2003**, *107*, 6176−6182.
(19) Jonsson, A. M.; Hallquist, M.; Ljungstrom, E. Impact of humidity on the ozone initiated oxidation of limonene, [delta]^3-carene, and [alpha]-pinene. *Environ. Sci. Technol.* **2006**, *40* (1), 188−194.
(20) Tolocka, M. P.; Saul, T. D.; Johnston, M. V. Uptake of nitric acid onto sodium chloride droplets using single-particle mass spectrometry. *J. Phys. Chem. A* **2004**, *108*, 2659−2665.
(21) Odum, J. R.; Jungkamp, T. P. W.; Griffin, R. J.; Flagan, R. C.; Seinfeld, J. H. The atmospheric aerosol-forming potential of whole gasoline vapor. *Science* **1997**, *276*, 96−99.
(22) Odum, J. R.; Hoffmann, T. R.; Bowman, F. M.; Collins, D.; Flagan, R. C.; Seinfeld, J. H. Gas/particle partitioning and secondary organic aerosol yields. *Environ. Sci. Technol.* **1996**, *30*, 2580−2585.
(23) Reents, W. D.; Ge, Z. Simultaneous elemental composition and size distributions of submicron particles in real time using laser atomization/ionization mass spectrometry. *Aerosol Sci. Technol.* **2000**, *33* (1−2), 122−134.
(24) Reents, W. D.; Schabel, M. J. Measurement of individual particle atomic composition by aerosol mass spectrometry. *Anal. Chem.* **2001**, *73* (22), 5403−5414.
(25) Park, K.; Lee, D.; Rai, A.; Mukherjee, D.; Zachariah, M. R. Size resolved kinetics measurements of aluminum nanoparticle oxidation by single particle mass spectrometry. *J. Phys. Chem. B* **2004**, *109*, 7290−7297.
(26) Oktem, B.; Tolocka, M. P.; Johnston, M. V. On-Line analysis of organic components in fine and ultrafine particles by photoionization aerosol mass spectrometry. *Anal. Chem.* **2004**, *76* (2), 253−261.
(27) Oktem, B.; Tolocka, M. P.; Zhao, B.; Wang, H.; Johnston, M. V. Role of aliphatic and aromatic hydrocarbons in soot nucleation and growth in a laminar premixed ethylene−oxygen−argon Flame. *Combust. Flame* **2004**, *142*, 364−373.
(28) Zahardis, J.; LaFranchi, B. W.; Petrucci, G. A. Photoelectron resonance capture ionization-aerosol mass spectrometry of the ozonolysis products of oleic acid particles: Direct measure of higher molecular weight oxygenates. *J. Geophys. Res.* **2005**, *110*, p. D08307 (doi: 10.1029/2004JD005336).
(29) Clark, R. J. H.; Foley, L. J. Photochemically induced reactions of ozone with 1,2-dibromoethene and 1,2-dichloroethene: An FT-IR matrix isolation study. *J. Phys. Chem. A* **2002**, *106* (14), 3356−3364.
(30) Bailey, P. S. *Ozonation in Organic Chemistry*, 1st ed.; Trahanovsky, W., Ed.; Academic Press: New York, 1978; p 272.
(31) Barton, M.; Ebdon, J. R.; Foster, A. B.; Rimmer, S. Complete ozonolysis of alkyl substituted ethenes at −60 °C: Distributions of ozonide and oligomeric products. *Org. Biomol. Chem.* **2005**, *3* (7), 1323−1329.
(32) Greenwood, F. L.; Rubinstein, H. Ozonolysis. IX. The alkene ozonation oligomer. *J. Org. Chem.* **1967**, *32*, 3369−3374.
(33) Barton, M.; Ebdon, J. R.; Foster, A. B.; Rimmer, S. Ozonolysis of tetramethylethylene: Characterization of cyclic and open-chain oligoperoxidic products. *J. Org. Chem.* **2004**, *69* (21), 6967−6973.
(34) Tobias, H. J.; Ziemann, P. J. Kinetics of the gas-phase reactions of alcohols, aldehydes, carboxylic acids, and water with the C13 stabilized Criegee intermediate formed from the ozonolysis of 1-tetradecene. *J. Phys. Chem. A* **2001**, *105*, 6129−6135.
(35) Creheut, R.; Anglada, J. M.; Bofill, J. M. Tropospheric formation of hydroxymethyl hydroperoxide, formic acid, H2O2, and OH from carbonyl oxide in the presence of water vapor: A theoretical study of the reaction mechanism. *Chem.—Eur. J.* **2001**, *7* (10), 2227−2235.
(36) Neeb, P.; Sauer, F.; Horie, O.; Moortgat, G. K. Formation of hydroxymethyl hydroperoxide and formic acid in alkene ozonolysis in the presence of water vapour. *Atmos. Environ.* **1997**, *31* (10), 1417−1423.
(37) Hasson, A. S.; Ho, A.; Kuwata, K.; Paulson, S. E. Production of stabilized Criegee intermediates and peroxides in the gas-phase ozonolysis of alkenes. 2. Asymmetric and biogenic alkenes. *J. Geophys. Res.* **2001**, *106* (D24), 34143−34153.
(38) Ryzhkov, A. B.; Ariya, P. A. A theoretical study of the reactions of carbonyl oxide with water in the atmosphere: The role of water dimer. *Chem. Phys. Lett.* **2003**, *367*, 423−429.
(39) Ryzhkov, A. B.; Ariya, P. A. A theoretical study of the reactions of parent and substituted Criegee intermediates with water and water dimer. *Phys. Chem. Chem. Phys.* **2004**, *6*, 5042−5050.
(40) Arey, J.; Atkinson, R.; Aschmann, S. M. Product study of the gas-phase reactions of monoterpenes with the hydroxyl radical in the presence of NO*x*. *J. Geophys. Res.* **1990**, *95*, 18539−18546.
(41) Hull, L. A.; Hisatsune, I. C.; Heicklen, J. Vapor-phase thermal decomposition of some simple ozonides. *J. Phys. Chem.* **1972**, *76* (19), 2659−2665.
(42) Ewing, J. C.; Church, D. F.; Pryor, W. A. Thermal decomposition of allylbenzene ozonide. *J. Am. Chem. Soc.* **1989**, *111*, 5839−5844.
(43) Jang, M.; Kamens, R. M. Newly characterized products and composition of secondary aerosols from the reaction of [alpha]-pinene with ozone. *Atmos. Environ.* **1999**, *33* (3), 459−474.
(44) Hasson, A. S.; Paulson, S. E. An investigation of the relationship between gas-phase and aerosol-borne hydroperoxides in urban air. *J. Aerosol Sci.* **2003**, *34*, 459−468.
(45) Djikaev, Y. S.; Bowles, R.; Reiss, H.; Hameri, K.; Laaksonen, A.; Vakeva, M. Theory of size dependent deliquescence of nanoparticles: Relation to heterogeneous nucleation and comparison with experiments. *J. Phys. Chem. B* **2001**, *105*, 7708−7722.

Received for review September 28, 2005. Revised manuscript received January 3, 2006. Accepted January 20, 2006.

ES051926F